Enhancing Broadband Vibration Energy Suppression Using Local Buckling Modes in Constrained Metamaterials

Ryan L. Harne[1]
Department of Mechanical and Aerospace Engineering, The Ohio State University, Columbus, OH 43210
e-mail: harne.3@osu.edu

Daniel C. Urbanek
Department of Mechanical and Aerospace Engineering, The Ohio State University, Columbus, OH 43210

Studies on dissipative metamaterials have uncovered means to suppress vibration and wave energy via resonant and bandgap phenomena through such engineered media, while global post-buckling of the infinitely periodic architectures is shown to tailor the attenuation properties and potentially magnify the effective damping effects. Yet, despite the promise suggested, the practical aspects of deploying metamaterials necessitates a focus on finite, periodic architectures, and the potential to therefore only trigger local buckling features when subjected to constraints. In addition, it is likely that metamaterials may be employed as devices within existing engineering systems, so as to motivate investigation on the usefulness of metamaterials when embedded within excited distributed or multidimensional structures. To illuminate these issues, this research undertakes complementary computational and experimental efforts. An elastomeric metamaterial, ideal for embedding into a practical engineering structure for vibration control, is introduced and studied for its relative change in broadband damping ability as constraint characteristics are modified. It is found that triggering a greater number of local buckling phenomena provides a valuable balance between stiffness reduction, corresponding to effective damping magnification, and demand for dynamic mass that may otherwise be diminished in globally post-buckled metamaterials. The concept of weakly constrained metamaterials is also shown to be uniformly more effective at broadband vibration suppression of the structure than solid elastomeric dampers of the same dimensions.
[DOI: 10.1115/1.4036888]

1 Introduction

The achievement of non-natural vibration and wave filtering characteristics in engineered material systems has motivated a host of recent research [1]. The exciting possibilities empowered by such metamaterials include bandgap tuning for elastic wave suppression [2,3], tuned-mass absorber effects for vibration reduction at targeted frequencies [4], and adaptive control of nonreciprocal wave propagation [5], among other energy-manipulating capabilities [6]. Capitalizing on such unprecedented system-level properties, great advancements may be made for numerous vibration, wave, and noise control applications, let alone for other contexts where transmitted elastic and acoustic energies are encountered [7].

Many of the phenomena exploited in such envisioned metamaterials involve reactive impedances that inhibit vibration or wave energy transmission on the basis of storing the dynamic energy in on-site local potentials or by tailoring metamaterial architectures to cultivate bandgaps. The phenomena are often narrowband in nature, thus providing considerably greater effectiveness at particular frequencies associated with the on-site resonant potentials [8,9] or with the bandgaps [10]. These capabilities contrast with leveraging resistive impedances that inhibit energy transmission via dissipative phenomena. Indeed, recent efforts have shown that traditional resonant- or bandgap-based metamaterials may still yield remarkable control of vibration and wave energy in the presence of internal dissipation mechanisms [11–14], although the general, complex mechanical impedance may be less effective at suppressing the vibration or wave energy at specific frequencies.

Taking a different perspective, rather than accommodate dissipative mechanisms in metamaterials alongside preferred reactive phenomena, researchers are recently taking advantage of nonlinearities in to realize unusual, broadband damping effects that are challenging to effect by resonant- or bandgap-based influences. For instance, a concept of "hyperdamping" has been proposed [15,16] and experimentally demonstrated [17]. These hyperdamping metamaterials leverage nonlinear, negative stiffness [18] via constraint mechanisms to reduce the fundamental stiffness to a critical point. At such critical points, the engineered microstructure transitions from pre- to post-buckling states such that dissipative restoring potentials dominate the interaction between the metamaterial and excitation mechanisms [19], yielding critically or overdamped behaviors in otherwise underdamped systems in absence of the constraints. Within an one-dimensional study and using an elastomeric metamaterial architecture, the authors experimentally uncovered [17] a 60% reduction of coefficient of restitution in drop tests by using the constrained, critical point metamaterials when compared to solid elastomer dampers; in addition, the metamaterials used 33% less mass than the solid elastomer demonstrating that the extreme dissipative mechanism can be used to great effect for one-dimensional wave energy control.

While the theoretical and experimental outcomes of the initial efforts on constrained metamaterials are promising, the reliance upon evidence from such simplified models and implementations to formulate conclusions does not necessarily assist to transition the concept from laboratory examination to engineering

[1]Corresponding author.

Contributed by the Technical Committee on Vibration and Sound of ASME for publication in the Journal of Vibration and Acoustics. Manuscript received January 2, 2017; final manuscript received May 10, 2017; published online July 26, 2017. Assoc. Editor: Stefano Lenci.

application, nor may the conclusions themselves translate. In particular, the study of one degree-of-freedom (DOF) and -dimensional systems and idealized structural implementations of the metamaterials in Ref. [17] lacks the complexity of drive and transfer impedances existing for multi-DOF and -directional systems in distributed structures [20]. Evaluating the distinct impedances probes the relative benefits of positioning vibration control implements since energy transfer paths are distinct and numerous for distributed parameter structures (e.g., beams, plates, etc.). Although envisioning a whole structure to be realized as the "metamaterial" is one way to closely connect theoretical study of a multi-DOF platform to final application [3], there is a likelihood that engineered metamaterials will find their way into use as vibration control devices that are retrofitted within existing structures in ways comparable to conventional damping materials and vibration absorbers [21,22]. This warrants studies having similar practical emphases including attention in the finite dimensions of the metamaterial itself [1,23].

In summary, there are clear needs to investigate emergent concepts of elastomeric metamaterials that exploit broadband damping phenomena with emphasis on multi-DOF or distributed parameter structures, whereby the relative advantages and disadvantages of the concepts may be more closely probed according to the unique transfer paths of vibration energy. While such scope is extensive by virtue of the myriad factors involved, this research aims to provide a first illumination of the effectiveness of using finite, constrained, elastomeric metamaterials to enhance broadband vibration energy suppression. Here, the structure whose vibrations are to be controlled is a distributed parameter structure that, while admittedly still fundamental in effect, is observed in many engineering applications ranging from civil, aerospace, marine, and automotive contexts, which improves the tenability of the research conclusions. The remainder of this paper reports complementary computational and experimental efforts undertaken to examine the influences of constraint mechanisms and placement strategies for harnessing engineered metamaterials as broadband dampers in the engineering structure. First, the metamaterial architecture is introduced and characterized for its mechanical properties. Then, an experimental setup is presented for its ability to investigate the more practical aspects of designing and deploying such metamaterials as embedded dampers. Finally, discussions of experimental and computational results are provided to elucidate how the emergent concepts may be appropriately capitalized upon when compared to traditional means for damping broadband vibrations in engineering structures.

2 Metamaterial Architecture and Characterization

Studies in elastomeric metamaterials have examined a breadth of periodic cellular architectures to evaluate each architecture's effectiveness for vibration and wave control [14,24]. In these examinations, the metamaterials have been presumed as infinite media in the span-wise dimensions. In this research, the realistic, limited span of the metamaterials is specifically accounted for, which has important ramifications on the insights drawn from the computational and experimental results.

The uncompressed metamaterial architecture considered here is shown in the top row of Fig. 1(*a*). The cross section of the metamaterial is constant through the thickness dimension which is the into-the-page dimension respecting the figure. The architecture is fabricated using silicone rubber (Smooth On Mold Star 15S) and three-dimensional printed molds. The periodic array of beams permits two manifestations of post-buckling: rotation and lateral deflection. To exemplify these behaviors and to characterize the mechanical properties of the metamaterials, experiments are conducted in a load frame (Mark-10 ES20 frame, PCB 1102-05A load cell, Micro-Epsilon ILD1700-200 laser displacement sensor). After several loading cycles to ensure that the specimens are at a consistent resting equilibrium, data of the compressive force and displacement of the metamaterial specimens are recorded (256 Hz sampling frequency, National Instruments and MATLAB data acquisition). Figures 1(*b*) and 1(*c*) present force–displacement and stiffness–displacement measurements, respectively, for three nominally identical metamaterial specimens labeled B1, B2, and B3. First, it is observed that the three specimens exhibit almost identical nuances of behavior throughout the loading sequences, indicating that the fabrication procedures are consistent, and the experimental protocols are sound. Second, the distinct manifestations of buckling are revealed. In Fig. 1(*c*) label 2, a sudden reduction in the instantaneous stiffness is measured consistently among the specimens, which occurs around displacement 0.7 mm. This is a sign of local buckling phenomena associated with minor rotation or lateral deflection of the beams within the constrained metamaterial architecture. Figure 1(*a*) part 2 highlights such features that may be manifested from one beam through a central core mass to another beam (e.g., the center post-buckled label and arrow), or may be evident solely along an individual beam (e.g., the rightmost post-buckled label and arrow). Additional realizations of the local buckling are clearly observed around displacement 1.2 mm, where the stiffness reduces again. Indeed, local buckling features are experimentally uncovered and visually evident throughout the

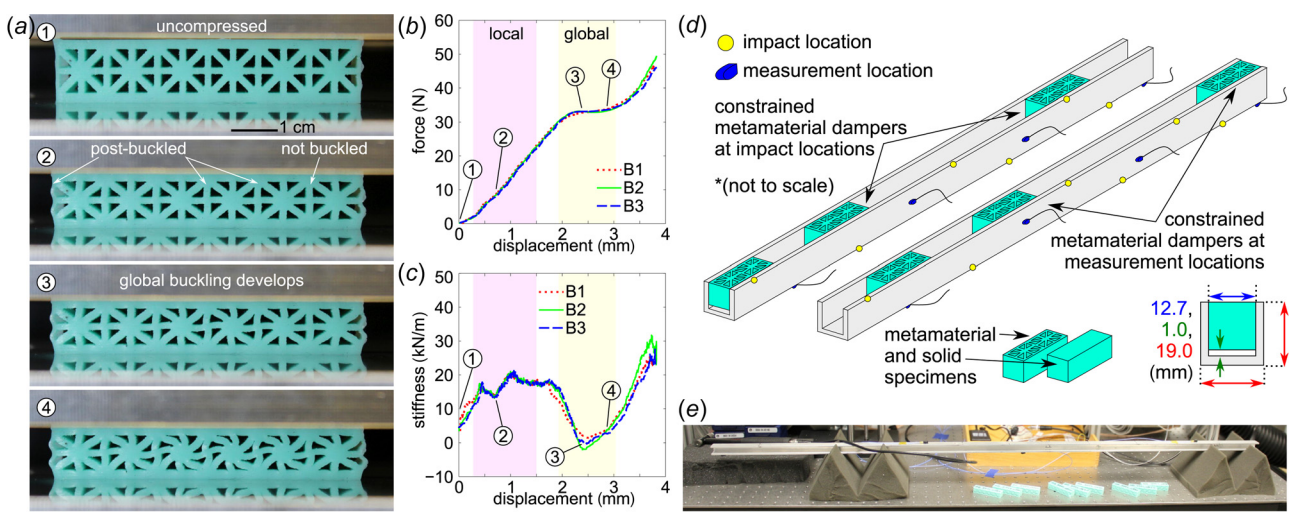

Fig. 1 (*a*) Metamaterial architecture subjected to compression, exhibiting local and global buckling behaviors; (*b*) load–displacement; (*c*) stiffness–displacement measurements for three nominally identical specimens; (*d*) schematic of impact hammer experiments on U-channel beam, comparison of metamaterial and solid specimens, and cross section dimensions of U-channel; and (*e*) photograph of experimental setup

constraint regime shown by the left highlight regions of Figs. 1(*b*) and 1(*c*). Such local buckling events have not been characterized before in the investigation of constrained metamaterials for broadband damping phenomena due to the attention on metamaterial architectures that do not possess such features [16,17].

The next manifestation of post-buckling is uncovered when the compressive displacement is near 2 mm, shown in Figs. 1(*b*) and 1(*c*). Around this extent of constraint, as shown in the photograph of Fig. 1(*a*) part 3, the lateral deflections of the beams become oriented so as to promote the rotational buckling mode that is characteristic of global buckling behavior. At the extremities of the metamaterial width, the lateral buckling mode persists due to the finite-ness of the system and free boundaries. The global buckling mode is associated with large reduction in the metamaterial instantaneous stiffness in the axis of compression that was evaluated previously for symmetric constrained metamaterials [16,17]. The large stiffness reduction, Fig. 1(*c*), is also that theoretically associated with the onset of the greatest damping effects due to the relative dominance of dissipative potentials since the elastic potentials are diminished [19]. For the finite-dimensioned metamaterial considered here, the global buckling behavior permeates through the architecture when the compressive displacement increases, as shown by the part 4 of Fig. 1(*a*) and with the corresponding labels in Figs. 1(*b*) and 1(*c*). Compaction occurs for further increase in the displacement beyond this regime.

Toward forming a broad perspective as to the effectiveness of constrained metamaterials for vibration damping when such devices are embedded into engineering structures, it is pertinent to study the influences of local buckling phenomena since they are numerous in finite, periodic metamaterials, e.g., appearing throughout the left highlighted regions in Figs. 1(*b*) and 1(*c*), and are inevitable in the practice of using nominal metamaterial specimens within realistic structures. Previous efforts gave attention to constrained metamaterials to compare the properties of uncompressed and post-buckled configurations using architectures that do not readily permit local buckling events [16,17,25]. Thus, the capability to harness local buckling features for vibration damping is specifically assessed in this research.

The engineering structure considered is a U-channel (or C-channel) beam with free boundary conditions. Beams of this geometry are encountered throughout civil, aerospace, marine, and automotive contexts, and the open geometry of the structure is amenable to the inclusion of damping materials, and in particular amenable for the constrained metamaterial examined here. A schematic of the beam with embedded metamaterial dampers is shown in Fig. 1(*d*). The beam is made of aluminum, has 1.22 m length, and has mass 524 g (McMaster-Carr, 9001K47). As shown in Fig. 1(*e*), the free supports are realized by foam wedges that hold the beam at arbitrary locations; the use of arbitrary support locations avoids suppressing vibration modes. Three metamaterial specimen types are fabricated, termed A, B, and C, and three specimens of each type are fabricated, such as the B1, B2, and B3 whose load-frame measurements are given in Figs. 1(*b*) and 1(*c*). The metamaterial cross section void geometry shown in Fig. 1(*a*) is used across all specimen types, while the overall height of each type varies in order to affect different extents of static compression within the U-channel that has a 12.7 mm height as shown in Fig. 1(*d*). Thus, the fabricated specimens A have a mean height 13.06 mm, B have height 13.48 mm, and C have height 13.71 mm. Respecting the 12.7 mm height of the U-channel structure and as supported by finite element (FE) modeling results presented in Sec. 2.1, the metamaterial specimen type A is constrained but not to an extent to induce local buckling events, type B is constrained on the verge of inducing local buckling, and type C is constrained to the extent that it induces numerous local (but not global) buckling features. As observed in Figs. 1(*b*) and 1(*c*), the instantaneous force and stiffness are both seen to undergo sudden drops in the regime of local buckling, which enhances the roles of dissipative potentials and hence damping properties. To assess the advantage of the metamaterial architecture respecting a baseline, the solid elastomer itself is fabricated to the same dimensions as the metamaterial specimens, excepting the height which is 12.85 mm, selected to as to held firmly within the U-channel but not be significantly compressed. As a result, the solid specimens are 36% more massive than the mean mass of the metamaterial specimens. The method of using such bulk damping materials as embedded into open channel beams is common in practice [22], so that this research may assess the relative advantage of exploiting the lighter-weight constrained metamaterial architecture in replacement of conventional solid material dampers.

2.1 Finite Element Modeling of the Constrained Metamaterial. While the load frame measurements shown in Figs. 1(*b*) and 1(*c*) and photographed in Fig. 1(*a*) reveal evidence of local buckling features, the existence of these phenomena are confirmed through FE modeling using COMSOL multiphysics. A two-dimensional plane strain model is constructed using a linear elastic material model of the silicone rubber with measured Young's modulus 752 kPa, measured density 1145 kg/m^3, and approximated Poisson's ratio 0.49. The exact cross-sectional geometry of the fabricated specimens is used in the FE model, and the compressive strain is realized in the identical manner as in experiments conducted with metamaterial specimens embedded within the beam. Namely, the top and bottom of the specimen along the height dimension are displaced inward according to the beam 12.7 mm height, which induces a static strain. Eigenfrequency studies are then undertaken since it is established that the eigenfrequency for a given vibration mode vanishes at the point of buckling [26].

The FE model results are presented in Fig. 2. For this finite-dimensioned metamaterial architecture, all of the lowest-order buckling modes are local. Indeed, similar to the experimental results, strains of 15–20% are required in the FE model to trigger global buckling (corresponding FE model results not shown). Several cases of eigenvalue veering are observed in the FE results of Fig. 2, while the local buckling mode points evident from 0% to 8.5% strain are highlighted. One particular local buckling mode, similar in topological deformation to the features of

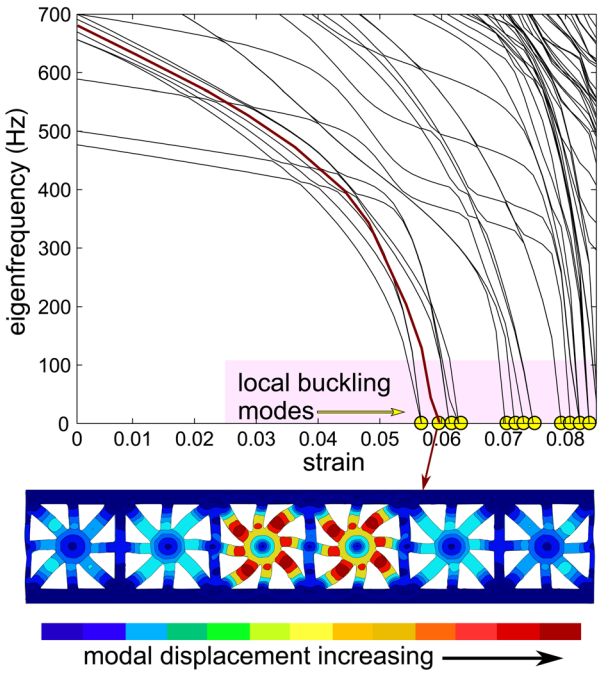

Fig. 2 FE model results of eigenfrequency change for change in compressive engineering strain. At bottom is an image of the deformation of a local buckling mode highlighted in the plot.

Fig. 1(*a*) part 2, is shown in the bottom of Fig. 2, which is found for strain around 6%. This local buckling mode reveals several instances of outer-most beam lateral deflection and minor rotational motion, yet only the inner-most pair of periodic unit cells undergoes appreciable rotation in this local buckling mode.

Considering the metamaterial specimen type heights with respect to the U-channel height, the static strain imposed on type A is approximately 2.7%, for B 5.8%, and for C 7.4%. Thus, to confirm the statement given in Sec. 2, the FE model results indicate that metamaterial specimens type A do not induce local buckling phenomena, although the specimens are certainly compressed within the beam. This contrasts with types B and C that are, respectively, on the verge of triggering local buckling and clearly induce many local buckling features. The ability for these critical mechanical properties of the architected metamaterials to govern the dissipation of dynamic vibration energies is next evaluated through experiments carried out with the specimens embedded in the beam structure.

3 Characterization of Broadband Vibration Energy Suppression

3.1 Experimental Results and Discussions. Modal hammer experiments are conducted on the U-channel to evaluate the global vibration response of the beam with and without embedded dampers, whether of the solid type or metamaterial types. A modal hammer (PCB 086C01) impacts the beam at six locations shown in Fig. 1(*d*). Impact is made at a 45-deg angle to each edge to inject motion into bending and torsional vibration modes. Four miniature accelerometers (PCB 352A24) are attached to the beam at locations selected so as to adequately measure the vibration modes below approximately 10 kHz, according to a FE model of the U-channel beam created and assessed in Sec. 3.2. The sampling frequency is sufficiently high, 131.072 kHz, to accurately capture the impact force from the modal hammer, and the data are collected and postprocessed using exponential windows to improve the quality of the acceleration to force transfer function (TF) computations [27]. For each configuration of the beam with or without embedded dampers, 90 TFs are averaged (from each of the four accelerometers) so that the global vibration response of the beam is determined from 360 measurements.

In applications of structural damping, placement of damping materials may be as important as selecting the appropriate materials themselves [20,22]. Thus, to evaluate the influences of applying the solid or metamaterial dampers within the beam to suppress the broadband, global vibration energy, two cases are considered, as schematically shown in Fig. 1(*d*). In one case, the dampers are embedded into the beam at the impact locations, while in the other case the dampers are positioned at locations coincident with the acceleration measurements. Note that in both cases, the solid or metamaterial dampers do not touch the bottom of the U-channel, as shown in Fig. 1(*d*), so as to provide a uniaxial contact with the beam. To ensure that the insights and conclusions are established upon sufficient diversity of data, two instances of such positioning are experimentally considered. Thus, four series of experiments are undertaken with any given damper set, i.e., impact locations 1, response measurement locations 1, impact locations 2, and response measurement locations 2.

The global vibration responses of the beam with and without the embedded dampers from the experiments of the first instance are shown in Fig. 3. Figures 3(*a*) and 3(*b*) show narrowband and one-third octave band evaluations, respectively, of the acceleration to force TF when the dampers are positioned at the impact locations, while Figs. 3(*d*) and 3(*e*) show the corresponding results when dampers are at response measurement locations. The different line styles in each figure denote measurements conducted with only the bare beam (dotted curve), with three solid damper specimens (dash-dot), with three metamaterial damper specimens of type A (thin solid), metamaterial type B (thick solid), and metamaterial type C (dash).

Considering the narrowband presentations of the data, the two lower order vibration modes around 200 Hz are not greatly suppressed by either the solid or metamaterial dampers, regardless of increasing metamaterial constraint (i.e., comparing types A, to B, to C). This is to be anticipated since the lower order vibration modes of distributed structures are associated with long standing wavelengths and large displacements. Using the FE model described in Sec. 3.2, Figs. 3(*a*) and 3(*d*) classify the type of the vibration mode for those modes with natural frequencies 1 kHz or

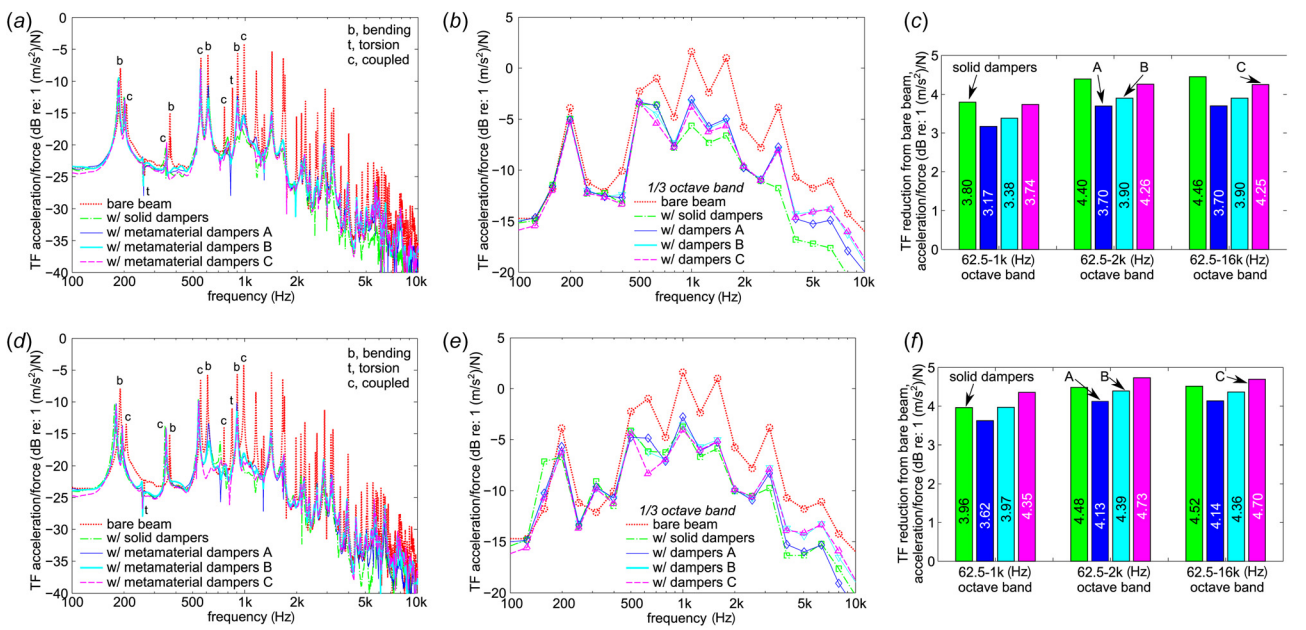

Fig. 3 Transfer function measurements of beam global acceleration to impact force. (*a*)–(*c*) present results for the instance where the embedded dampers are positioned at the impact locations, while (*d*)–(*f*) present results when the embedded dampers are positioned at response measurements locations. (*a*) and (*d*) provide narrowband plots, (*b*) and (*e*) provide one-third octave band plots, and (*c*) and (*f*) provide octave band totals of TF reductions from the case of the global vibration of the bare beam.

less, whether bending "b," torsional "t," or a mode that couples bending and torsion "c." These lower-order modes around 200 Hz are both associated with bending and/or torsional displacements significantly greater than the largest dimension of the metamaterials or solid dampers. To most effectively suppress such vibrations using small amount of mass requires mostly reactive impedances [20] like tuned vibration absorbers [9], rather than general resistive and reactive impedances exemplified in the metamaterial dampers examined here. Consequently, the modes around 200 Hz exhibit mostly mass-loading by the downward shift in resonant peaks once the solid or metamaterial dampers are embedded in the beam. The mass-loading is admittedly not large because the metamaterial dampers constitute just 6% mass of the overall U-channel.

On the other hand, at frequencies greater than about 500 Hz, numerous and considerable influences on the beam global vibration response are observed due to the embedded dampers. These vibration modes are variously associated with bending, torsion, or coupled behaviors, as labeled in Figs. 3(*a*) and 3(*d*). Giving attention first to the measurements when dampers are placed at the impact locations, Fig. 3(*a*), it is found that both solid and metamaterial dampers suppress resonances by about 10 dB or more above 700 Hz, while the pair of resonances near 600 Hz are attenuated to different extents based on the damper type. For instance, in the one-third octave band evaluation, Fig. 3(*b*), the solid and metamaterial A dampers suppress approximately the same global vibration energy from the hammer impacts in the 625 Hz band, while the increase of constraint on the metamaterial from type A to type B and then to type C reveals an increasing ability for the metamaterial to attenuate the vibration. This is evidence that capitalizing on the local buckling features, by using greater constraints on the metamaterial architecture, gives rise to greater damping capability in this lower frequency band.

At higher frequencies, such as above 700 Hz, all of the dampers adequately attenuate the narrowband resonances, although the overall levels of the TFs reduce considerably. This suggests that achieving such vibration suppression would not result in large practical influence due to the minor contribution of this bandwidth to the global beam response. To evaluate this statement, Fig. 3(*c*) shows the reduction in the TF achieved by the different dampers at the impact locations compared to the bare beam alone, and computed over the octave band ranges indicated. While almost 0.5 dB difference is uniformly observed comparing the 62.5–1 kHz octave bands to the 62.5–2 kHz evaluation, there are insignificant changes in the overall TF reduction in the 62.5–16 kHz octave bands compared to the 62.5–2 kHz, indicating that a bulk of the kinetic energy of the impacted U-channel exists at frequencies 2 kHz and less. Yet, importantly, it is found across all octave band ranges that increased metamaterial constraint increases the global reduction of the TF. In fact, the metamaterial type C specimens are seen to provide comparable overall attenuation of the broadband vibration energy of the beam as the solid dampers, i.e., within 0.15 dB.

Comparing the narrowband TFs when the dampers are placed at the impact locations, Fig. 3(*a*), to when the dampers are placed at the response measurement locations, Fig. 3(*d*), it is not immediately apparent which placement approach is more effective at suppressing the overall beam vibration. In particular within the bandwidth around 700–2 kHz, there are resonances that are greatly attenuated in one instance but not the other. The one-third octave band evaluation, Fig. 3(*e*), reveals that the increased constraint enhances the global vibration suppression of the 625 Hz band when the metamaterial dampers are positioned at the response measurement locations, which is in agreement with the results found when the same dampers are at impact locations. Thus, by capitalizing on increased local buckling phenomena in the metamaterial specimens C, greater broadband damping of the U-channel vibrations is achieved. Considering the octave band evaluations in Figs. 3(*c*) and 3(*f*), the TF reductions exhibit a statistically significant increase, around 0.5 dB, by positioning the

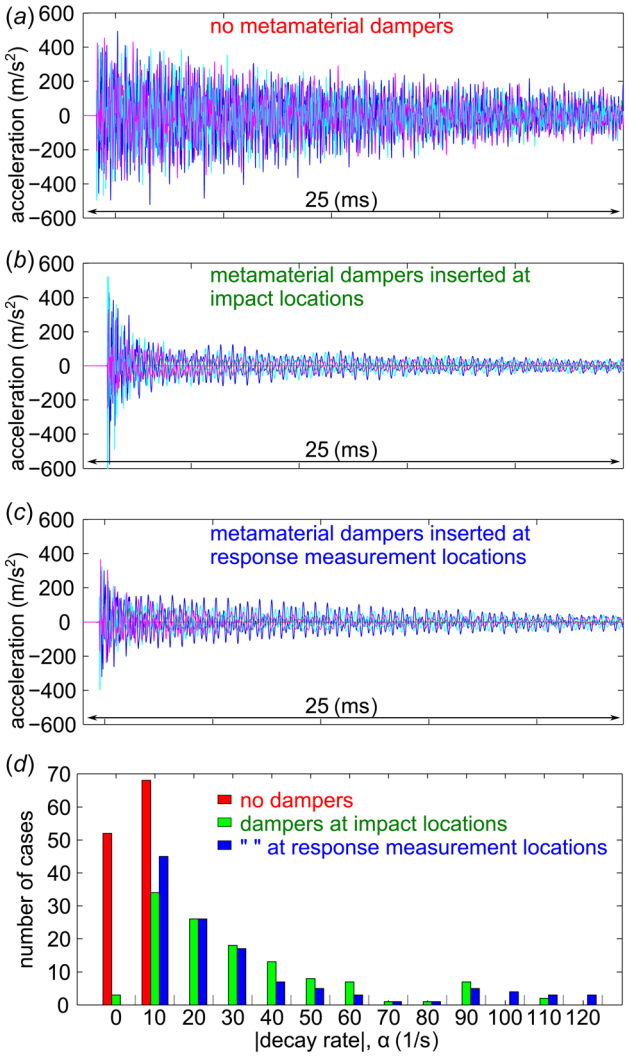

Fig. 4 Representative time series of acceleration ring-down responses after hammer impact. Beam acceleration from the four accelerometers shown for the beam with (*a*) no dampers embedded, with (*b*) metamaterial dampers type C at impact locations, and with (*c*) metamaterial dampers type C at response measurement locations. (*d*) The exponential decay rates computed from three representative experimental series.

metamaterial dampers at response measurement locations compared to the impact locations, although the general trends of constraint on the TF reduction are consistent regardless of positioning. Studying the outcomes of the second experimental instance of positioning, presented in the following paragraphs, helps to ultimately assess the effectiveness of solid and constrained metamaterial dampers in a statistically meaningful way.

To look more deeply into the influences of applying the dampers at different locations for global vibration suppression, Fig. 4 presents representative acceleration time series after hammer impact and data analysis to evaluate the rate of decay of the beam acceleration response envelopes. First considering the time series, it is clear that embedding the metamaterial dampers type C at either of the location region, Figs. 4(*b*) and 4(*c*), provides a considerable and rapid attenuation of the beam acceleration when compared to the beam without dampers, Fig. 4(*a*). Then, using all of the data from experimental measurements that contained 120 individual impacts, Fig. 4(*d*) presents the results of the distribution of exponential envelope decay rates, according to fits of $|\bar{w}(t)| = \beta e^{-\alpha t}$, where $|\bar{w}(t)|$ is the envelope of an acceleration time series, β is an amplitude constant, and α is the decay rate.

Table 1 Decay rate mean and standard deviation for the data presented in Fig. 4(*d*)

Exponential decay rate in system after hammer impact	|Decay rate| mean (1/s)	Decay rate standard deviation (1/s)
No specimen	5.002	1.006
Metamaterial dampers at impact locations	30.12	25.44
metamaterial dampers at response measurement locations	30.89	31.81

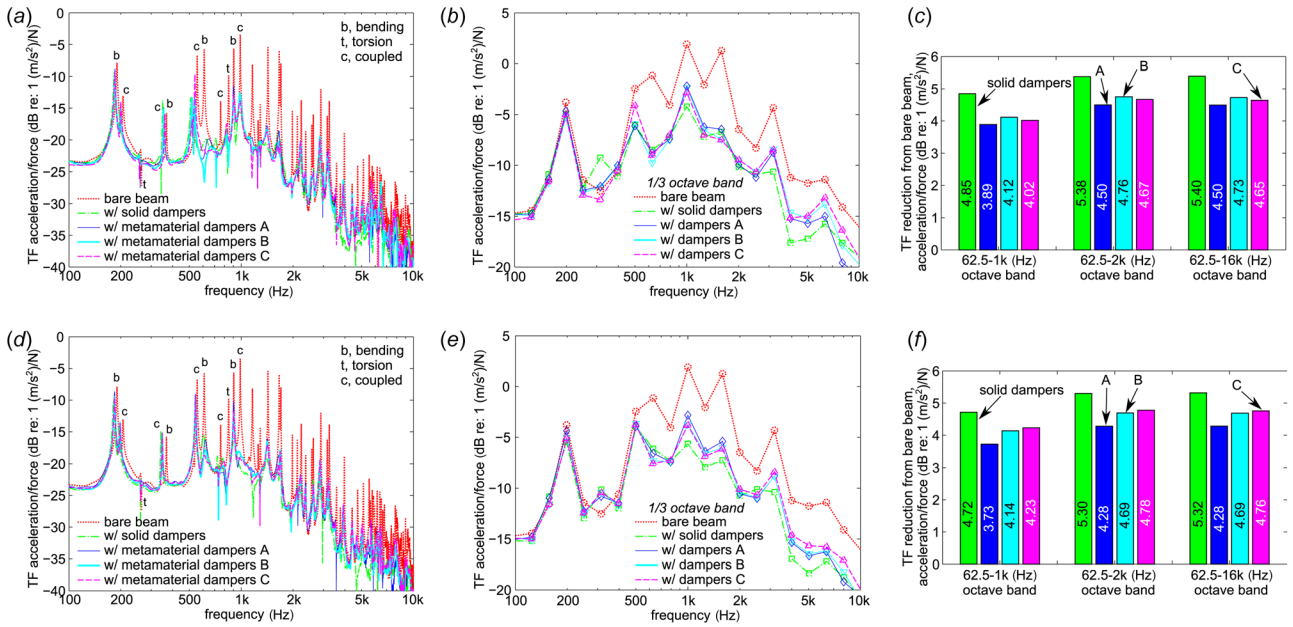

Fig. 5 Transfer function measurements of beam global acceleration to impact force. Data obtained for the second instance of impact location and response measurement location experimentally considered. Layout of subfigure parts and presentation are identical to those in Fig. 3.

Higher values of decay rate indicate more rapid suppression of the transient vibration. Considering the statistical results of Fig. 4(*d*), it is clear that there is tremendous increase in the decay rate by applying the metamaterial dampers. It is also clear that there is no significant difference between applying the dampers at the impact locations or at the response measurement locations based on the distribution of the decay rates. Table 1 consolidates the statistics from the plot of Fig. 4(*d*), and confirms the minor difference between the metamaterial placements on the ultimate outcome of the vibration attenuation. While not exactly an example of reciprocity due to the six impact locations, four measurement locations, and three dampers for each damper type and experimental instance evaluated, such equivalence of outcome suggests that the use of constrained metamaterial dampers provides a certain global "drain" of vibration energy in excited engineering structures that have relatively few pathways of energy transfer through them, regardless of where the dampers are positioned.

Data and evaluations of the global TF for the second instances of impact and response measurement location placement for the dampers are shown in Fig. 5, using the same layout and data presentation methods as in Fig. 3. Comparing the plots, the narrowband results change only in nuanced ways: certain resonances more greatly attenuated for the first instance in Figs. 3(*a*) and 3(*d*) according to specific damper type and placement may have different counterpart resonances that are greatly attenuated in Figs. 5(*a*) and 5(*d*) in the second instance. This is borne out comparing the one-third octave band evaluations in Figs. 3(*b*), 3(*e*), 5(*b*), and 5(*e*), where the distribution of attenuation in the one-third octave bands is found to shift only slightly from one instance to the other in accordance with the damper positioning changes. Interestingly, the 625 Hz one-third octave band in the second instance, Figs. 5(*b*) and 5(*e*), also reveal clear dependence on the constraint applied to the metamaterial dampers. Yet, for the second instance of damper placement at the impact location, Fig. 5(*b*), the moderately constrained metamaterial type B is more effective at reducing the TF than the more constrained metamaterial type C that triggers a greater number of the local buckling modes. Considering these trends of Figs. 3(*a*), 3(*d*), 5(*a*), and 5(*d*) in light of the classification of each vibration mode as related to bending, torsion, or a coupling of the U-channel dynamic behaviors, there does not appear to be clear connection between the significance of mode suppression and the type of mode attenuated. Indeed, for a vibration control implement that capitalizes on resistive impedance for broadband frequency effect, like the local buckling and damping phenomena exploited in this research, it is logical that the metamaterials will not especially tackle one type of mode than another.

Two notable distinctions are seen between the two instances of damper placement. First, in the second instance considered, Figs. 5(*c*) and 5(*f*) show that the solid dampers are more effective at TF suppression than the constrained metamaterial dampers. The second distinction is reported in the prior paragraph and is clear in Fig. 5(*c*): for impact location placement, the metamaterial type B is more effective at reducing the TF than the type C that triggers a greater number of the local buckling modes and thus hypothetically should exhibit a greater enhancement of damping properties. This contrasts with the results of the first instance, Fig. 3(*c*), where the more constrained type C metamaterial damper provided the greatest overall reduction to the acceleration to force TF. Yet, the statistics of the TF reductions taken from all of the experimental data evaluations in Figs. 3(*c*), 3(*f*), 5(*c*), and 5(*f*) suggests a general conclusion may be reached. Table 2 presents the mean TF reductions from the global vibration response of the bare beam, where the mean is taken over the two instances as well as over the two cases of impact location and response measurement location placement for the dampers. Also shown in parentheses in Table 2

Table 2 Mean TF reduction from bare beam global vibration computed as mean of all instances and all cases of damper placement

	Mean TF reduction from bare beam global vibration response (dB) (TF reduction per mass (dB/g))			
Octave band total (kHz)	Solid dampers	Metamaterial A	Metamaterial B	Metamaterial C
62.5–1	4.33 (0.286)	3.60 (0.325)	3.91 (0.352)	4.09 (0.368)
62.5–3	4.89 (0.323)	4.15 (0.374)	4.44 (0.400)	4.61 (0.415)
62.5–16	4.92 (0.325)	4.15 (0.374)	4.42 (0.398)	4.14 (0.414)

Note: Computed are the mean reductions and the mean reductions per damper mass.

are the TF reductions per damper mass. In all octave bands considered, metamaterial C, having the greatest constraint and exhibiting the most local buckling features, reveals the greatest overall attenuation of the beam vibration energy per mass. The absolute, broadband vibration suppression of metamaterial C is within 0.7 dB of the solid dampers, while an average enhancement of 28% of the attenuation per mass compared to the solid dampers is realized using this constrained metamaterial. These results confirm the hypothesis of this research that leveraging greater numbers of local buckling modes via static metamaterial constraints empowers large enhancement of damping properties; in other words, the TF reduction per mass is increased although less absolute mass is utilized via the metamaterials.

3.2 Finite Element Modeling of Metamaterial Damping Impact on Beam Vibration. The insights reached by the experimental undertaking encourage an investigation into the limits of the trends that continually increase damping properties, cultivated by triggering the local (and ultimately the global) modes of post-buckling in the metamaterial, promote greater suppression of the beam structure vibration. To this end, the finite element model is built upon to account for the exact three-dimensional U-channel beam geometry, hammer excitation locations, and metamaterial damper placements. From preliminary efforts, it is found that including the exact metamaterial damper geometries in the model, as embedded within the U-channel beam, results in a computationally infeasible number of elements upon which matrix operations must be taken by the FE method solution process. This concern is due to the severe variation in length scales involved, from less than 1 mm for the metamaterial geometric features to greater than 1 m of the U-channel length, which results in a demand to finely mesh the whole geometry so as to avoid ill-conditioned matrices associated with large mismatch between mesh densities.

As a result, the metamaterial damper geometries are not explicitly defined in the FE model. Instead, the influences of the metamaterials are accounted for via distributed impedances that exert time-harmonic forces on the beam inner channel surfaces where the metamaterials are placed in the experiments. In addition to the computational infeasibility of using the exact metamaterial geometry, the rationale for modeling the metamaterial dampers as only impedances is that their role is to provide broadband damping that may be, in a first approximation, simplified to resistive and reactive impedance components in one dimension, like the stiffness–displacement measurements of Fig. 1(*c*) encourage. Thus, based on the FE model outcomes respecting observations from the prior experiments, one is able to evaluate how comparable are the influences of constrained metamaterial dampers on the U-channel beam to a single-DOF representation. Consequently, the impedance representation of the lowest-order dynamic response of the metamaterials is given by

$$Z_m = j\omega m \frac{\omega_n^2 + j2\zeta\omega_n\omega}{\left(\omega_n^2 - \omega^2\right) + j2\zeta\omega_n\omega} \tag{1}$$

where m is the dynamic mass of the metamaterial (here assumed to be the collective mass of beam intersection points of the metamaterial damper geometry, which is approximately one-eighth of the overall metamaterial mass), $\omega_n/2\pi$ is the natural frequency of the principal motion of the metamaterial (here taken to be 100 Hz, considering the local buckling states to have very small natural frequency, although the FE results are found to be insensitive to this frequency so long as the value is less than around 200 Hz), ω is the angular frequency of a harmonic excitation at the hammer excitation points, and $j = \sqrt{-1}$. The damping ratio ζ is taken as a parameter to vary in order to study the roles of damping properties change on the ability for the metamaterials to suppress the global vibration of the beam structure. Thus, increase in ζ is similar to triggering greater numbers of local buckling modes, by virtue of the effective metamaterial stiffness reductions, Fig. 1(*c*), to the point that global buckling may be triggered comparable to near-critical damping. As shown in Ref. [17], the exact value of the effective metamaterial damping ratio is dependent upon the baseline value of the unconstrained architecture, although damping ratio growth by two orders of magnitude is feasibly for constraint at a global buckling point.

As a first check, the natural frequencies of the bare U-channel beam determined from the FE model and those measured experimentally are contrasted. The average root-mean-square error between these measured and predicted natural frequencies from 100 to 1 kHz is just 2.41%, while the maximum absolute error is 3.11%. Figure 6 presents the FE model results, computed in one-third octave bands, when the metamaterials are placed at (a) the impact/excitation locations and (b) at the response measurement locations. The TF evaluations shown in the plots are computed in the same ways as performed experimentally in this work. Comparisons of the one-third octave band frequency distributions between the bare beam FE model results Figs. 6(*a*) and 6(*b*) (red dashed) and the experimental measurements in Figs. 3(*b*) and 6(*e*) or 5(*b*) and 5(*e*) (red dashed) show that the model is relatively successful to replicate the measured broadband response of the U-channel.

Considering the FE model results in Fig. 6, when the metamaterials are significantly underdamped, $\zeta = 0.001$, the locations of the narrowband resonances are primarily shifted or not affected at all, which has the consequence to redistribute the TF peaks in the one-third octave band representation. This result is consistent for both metamaterial placement cases from (*a*) to (*b*). Yet, as the damping grows to $\zeta = 0.01$ and then further to $\zeta = 0.1$, the results of the global vibration TF change dramatically. The growth of the effective damping property of the embedded metamaterials to $\zeta = 0.1$ results in a broadband dissipation effect by virtue of a reduction of the one-third octave band TF across nearly all frequencies considered, and this outcome is consistent whether the metamaterials are positioned at the impact locations, Fig. 6(*a*), or at the response measurement locations, Fig. 6(*b*). Indeed, this broadband damping effects occurs without any change in the metamaterial mass that would otherwise provide greater authority for the dampers to suppress the beam vibration. While this may suggest that never-ending growth of damping is desirable, in fact the FE model shows that the further increase of the damping ratio to $\zeta = 1$ is adverse to suppressing the broadband vibration energy of the beam. The results show that, regardless of metamaterial placement, considering both Figs. 6(*a*) and 6(*b*), the critically damped metamaterial with

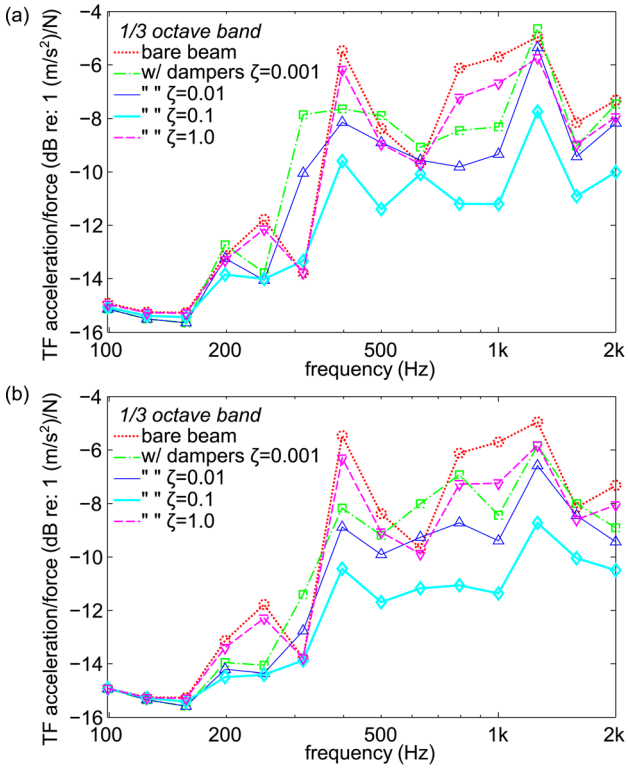

Fig. 6 FE model results of one-third octave band global acceleration to force TF, considering the metamaterial dampers to possess ranges of damping ratios, from significant underdamping to critical damping. Results shown for metamaterials at (*a*) impact locations and (*b*) response measurement locations (see color figure online).

$\zeta = 1$ provides significantly less TF reduction than the strongly, but still moderately, damped metamaterial with $\zeta = 0.1$. This result is due to the fact that the critically damped metamaterial is less inertially responsive and thus acts more like lumped mass at the locations where the metamaterial impedances interact with the beam.

These results are in clear qualitative agreement with the experiments. Specifically, the data show that leveraging enhanced constraints that promote more local buckling phenomena and provide softening stiffness, Fig. 1(*c*), and corresponding one-dimensional damping enhancement lead to increased suppression of broadband vibration. The FE model results corroborate this general conclusion and highlight that taking the concept to a further extreme, with critical damping, diminishes the advantageous broadband vibration control effect. Consequently, by virtue of a sufficient but not extreme damping magnification, it can be concluded that the local buckling modes of strategically constrained metamaterials are prime to be exploited for enhancement of broadband vibration energy attenuation capabilities when such devices are embedded into practical structures in operational conditions.

4 Conclusions

This research investigated the premise that the local modes of buckling in finite, periodic, constrained metamaterials are valuable phenomena to be leveraged toward the attenuation of broadband vibration energy in practical engineering structures. Through computational and experimental efforts, it is shown that greater activation of local buckling features uniformly enhances the ability for constrained elastomeric metamaterials to suppress vibrations of a beam structure into which the metamaterials are embedded. This outcome is consistent across a broad range of frequencies where the standing wavelengths are shorter than the order of magnitude of the structure length. It is also shown that the overall reduction of the global vibration response per mass is enhanced by about 30% via using the constrained metamaterials, when compared to using solid elastomeric dampers of the same dimensions. It is also demonstrated that the fundamental dynamic interaction between the metamaterial and host structure is comparable to a one-dimensional complex impedance that includes a reactance with low natural frequency and large but not overwhelming resistance, which provides a starting point for future, efficient modeling investigations. As a result, this research provides a first illumination that harnessing local buckling phenomena in finite metamaterial architectures is a concept able to be capitalized upon for controlling the vibrations of distributed and multidimensional structures encountered in numerous engineering contexts.

Acknowledgment

This research was supported in part by The Ohio State University Simulation Innovation and Modeling Center through a gift from Honda R&D Americas, Inc. The authors acknowledge Justin Bishop at The Ohio State University (OSU) for preliminary experiments and Martyn Morrish of Honda R&D Americas, Inc., for helpful conversations that collectively helped to stimulate this research. R. L. H. also acknowledges start-up funds from the Department of Mechanical and Aerospace Engineering at OSU.

References

[1] Cummer, S. A., Christensen, J., and Alù, A., 2016, "Controlling Sound With Acoustic Metamaterials," Nat. Rev., **1**, p. 16001.
[2] Liu, Y., Shen, X., Su, X., and Sun, C. T., 2016, "Elastic Metamaterials With Low-Frequency Passbands Based on Lattice System With on-Site Potential," ASME J. Vib. Acoust., **138**(2), p. 021011.
[3] Liu, X. N., Hu, G. K., Sun, C. T., and Huang, G. L., 2011, "Wave Propagation Characterization and Design of Two-Dimensional Elastic Chiral Metacomposite," J. Sound Vib., **330**(11), pp. 2536–2553.
[4] Chen, J. S., and Wang, R. T., 2014, "Wave Propagation and Power Flow Analysis of Sandwich Structures With Internal Absorbers," ASME J. Vib. Acoust., **136**(4), p. 041003.
[5] Popa, B. I., and Cummer, S. A., 2014, "Non-Reciprocal and Highly Nonlinear Active Acoustic Metamaterials," Nat. Commun., **5**, p. 3398.
[6] Haberman, M. R., and Guild, M. D., 2016, "Acoustic Metamaterials," Phys. Today, **69**(6), pp. 42–48.
[7] Hussein, M. I., Leamy, M. J., and Ruzzene, M., 2014, "Dynamics of Phononic Materials and Structures: Historical Origins, Recent Progress, and Future Outlook," ASME Appl. Mech. Rev., **66**(4), p. 040802.
[8] Nouh, M., Aldraihem, O., and Baz, A., 2014, "Vibration Characteristics of Metamaterials Beams With Periodic Local Resonances," ASME J. Vib. Acoust., **136**(6), p. 061012.
[9] Baravelli, E., and Ruzzene, M., 2013, "Internally Resonating Lattices for Bandgap Generation and Low-Frequency Vibration Control," J. Sound Vib., **332**(25), pp. 6562–6579.
[10] Huang, G. L., and Sun, C. T., 2010, "Band Gaps in a Multiresonator Acoustic Metamaterial," ASME J. Vib. Acoust., **132**(3), p. 031003.
[11] Hussein, M. I., and Frazier, M. J., 2013, "Metadamping: An Emergent Phenomenon in Dissipative Metamaterials," J. Sound Vib., **332**(20), pp. 4767–4774.
[12] Ba'ba'a, H. A., and Nouh, M., 2017, "An Investigation of Vibrational Power Flow in One-Dimensional Dissipative Phononic Structures," ASME J. Vib. Acoust., **139**(2), p. 021003.
[13] Shan, S., Kang, S. H., Wang, P., Qu, C., Shian, S., Chen, E. R., and Bertoldi, K., 2014, "Harnessing Multiple Folding Mechanisms in Soft Periodic Structures for Tunable Control of Elastic Waves," Adv. Funct. Mater., **24**(31), pp. 4935–4942.
[14] Shim, J., Wang, P., and Bertoldi, K., 2015, "Harnessing Instability-Induced Pattern Transformation to Design Tunable Phononic Crystals," Int. J. Solids Struct., **58**, pp. 52–61.
[15] Antoniadis, I., Chronopoulos, D., Spitas, V., and Koulocheris, D., 2015, "Hyper-Damping Peroperties of a Stiff and Stable Linear Oscillator With a Negative Stiffness Element," J. Sound Vib., **346**, pp. 37–52.
[16] Harne, R. L., Song, Y., and Dai, Q., 2017, "Trapping and Attenuating Broadband Vibroacoustic Energy With Hyperdamping Metamaterials," Extreme Mech. Lett., **12**, pp. 41–47.
[17] Bishop, J., Dai, Q., Song, Y., and Harne, R. L., 2016, "Resilience to Impact by Extreme Energy Absorption in Lightweight Material Inclusions Constrained Near a Critical Point," Adv. Eng. Mater., **18**(11), pp. 1871–1876.
[18] Kochmann, D. M., 2014, "Stable Extreme Damping in Viscoelastic Two-Phase Composites With Non-Positive-Definite Phases Close to the Loss of Stability," Mech. Res. Commun., **58**, pp. 36–45.
[19] Virgin, L. N., and Wiebe, R., 2013, "On Damping in the Vicinity of Critical Points," Philos. Trans. R. Soc. A, **371**(1993), p. 20120426.

[20] Fahy, F., and Gardonio, P., 1987, *Sound and Structural Vibration: Radiation, Transmission and Response*, Academic Press, Oxford, UK.
[21] Cremer, L., Heckl, M., and Petersson, B. A. T., 2005, *Structure-Borne Sound: Structural Vibrations and Sound Radiation at Audio Frequencies*, Springer, Berlin.
[22] Ungar, E. E., 1992, "Structural Damping," *Noise and Vibration Control Engineering*, L. L. Beranek, and I. L. Ver, eds., Wiley, New York.
[23] Celli, P., and Gonella, S., 2014, "Laser-Enabled Experimental Wavefield Reconstruction in Two-Dimensional Phononic Crystals," J. Sound Vib., **333**(1), pp. 114–123.
[24] Overvelde, J. T. B., and Bertoldi, K., 2014, "Relating Pore Shape to the Non-Linear Response of Periodic Elastomeric Structures," J. Mech. Phys. Solids, **64**, pp. 351–366.
[25] Wang, P., Casadei, F., Shan, S., Weaver, J. C., and Bertoldi, K., 2014, "Harnessing Buckling to Design Tunable Locally Resonant Acoustic Metamaterials," Phys. Rev. Lett., **113**(1), p. 014301.
[26] Virgin, L. N., 2007, *Vibration of Axially Loaded Structures*, Cambridge University Press, Cambridge, UK.
[27] Avitabile, P., 2001, "Experimental Modal Analysis: A Simple Non-Mathematical Presentation," Sound Vib., **35**(1), pp. 20–31.